Excitation mechanisms in moderate-energy Li^+-Ne collisions

S. Kita,[1] S. Gotoh,[1] N. Shimakura,[2] and S. Koseki[3]
[1]*Department of Systems Engineering, Nagoya Institute of Technology, Gokiso, Showa-ku, Nagoya 466-8555, Japan*
[2]*Department of Chemistry, Faculty of Science, Niigata University, Ikarashi, Niigata 950-2181, Japan*
[3]*Chemistry Department for Materials, Faculty of Engineering, Mie University, 1515 Kamihara, Tsu 514-0008, Japan*
(Received 10 December, 1998; revised manuscript received 26 April 2000; published 10 August 2000)

Excitation processes in Li^+-Ne collisions have been studied over a wide range of laboratory angles of $2° \leqslant \theta \leqslant 92°$, and at laboratory collision energies of $200 \leqslant E_{lab} \leqslant 500$ eV, by means of differential energy-transfer measurements. One- and two-electron excitations for both charge-exchange reactions and direct excitations of the Ne atoms were observed at reduced laboratory angles of $E_{lab}\theta > 6$ keV deg. The electronic transitions take place through diabatic potential crossings at internuclear distances of $R \leqslant 0.57$ Å. The excitation mechanisms near threshold have been investigated by referring to *ab initio* potentials, and the mechanisms of dominant one- and two-electron excitations could be well understood. Analysis of the theoretical potentials suggests that one-electron excitations are due to avoided-crossing interactions, while two-electron excitation occurring through two successive one-electron transitions can be interpreted by a combination of avoided-crossing and noncrossing interactions.

PACS number(s): 34.50.Fa, 34.20.Cf

I. INTRODUCTION

Through numerous experimental and theoretical studies on excitation processes, an understanding of the excitation mechanisms in slow collisions of heavy particles has been well enhanced in the last several decades. The excitations predominantly proceed through nonadiabatic radial couplings, which are classified into avoided-crossing interactions and noncrossing interactions [1]. The excitation processes in slow collisions are generally interpreted with a quasimolecular framework. If two particles approach each other to a distance shorter than a critical distance R_c, an excited quasimolecule is temporarily formed with a certain probability.

Excitations in moderate-energy collisions between closed-shell particles have long been studied by employing several experimental methods [2–13]. Excitation probability strongly depends on colliding system. Transitions occurring through avoided crossings in symmetric and quasisymmetric closed-shell systems have a large probability [7–10], while transitions due to noncrossing interactions in most asymmetric closed-shell systems have a very small probability [11–13]. Despite a large amount of earlier studies, such a strong system dependence of the excitations has not yet been fully interpreted.

Differential scattering of Li^+ ions from Ne atoms was studied experimentally and theoretically by Barat *et al.* [11]. In their experiments, an energy analysis of the Li^+ ions was performed to obtain doubly differential cross sections (DCS's), while for Li atoms produced by charge transfers only the total DCS was measured without energy analysis. Thus the excitation mechanisms in the Li^+-Ne collisions have not been sufficiently understood. In this study, we have carried out a translational-energy analysis of all the particles scattered in the Li^+-Ne collisions (Li^+, Li, Ne, and Ne^+) by using a time-of-flight technique, and the DCS's for all the scattered particles have been measured at laboratory collision energies of $200 \leqslant E_{lab} \leqslant 500$ eV and scattering angles of $2° \leqslant \theta \leqslant 92°$. The experimental DCS's have been analyzed by assuming diabatic potentials for the ground and excited states. The diabatic potentials provide classical trajectories of particles. The diabatic potential parameters which characterize electronic transitions, at the crossing distance R_c, have been evaluated through the analysis.

In this study, electronic energies $E(R)$'s for the ground and excited states of $(LiNe)^+$ have also been calculated using a multiconfiguration self-consistent field (MCSCF) method [14]. Electronic transitions due to radial coupling take place efficiently around the critical (crossing) distance R_c, where the adiabatic difference potential $\Delta E = E_j - E_i$ between interacting states i and j has a minimum value ΔE_{min} [11,13,15]. Around the distance R_c, electronic configurations in the wave functions interchange with each other between interacting states in the avoided-crossing case, while there is no change of configurations in the noncrossing case. By evaluating diabatic potential parameters at R_c from the MCSCF potentials, we have obtained information on the excitation mechanisms for the dominant excitation processes near threshold angles.

In Li^+-Ne collisions, two-electron ($2e$) excitations as well as one-electron ($1e$) excitations have been observed with remarkable probability. The $2e$ excitation into the Li^+-Ne ($3s^2$) state was interpreted to take place through two successive $1e$-transition processes, similarly to that in the Na^+-Ne collisions [9,10(b)], i.e., $Ne \rightarrow Ne(3s) \rightarrow Ne(3s^2)$, rather than a simultaneous $2e$ transition, $Ne \rightarrow Ne(3s^2)$. An analysis of the MCSCF calculations shows that the first process in the two successive $1e$ transitions is attributed to the avoided crossing. On the other hand, around the second transition point no interchange of the electronic configurations is recognized, so the second process is attributed to the noncrossing interaction.

II. EXPERIMENTS

A. Apparatus

Differential scattering experiments have been performed using a crossed-beam apparatus. Details of the apparatus were given elsewhere [16] (and a schematic drawing of the apparatus is presented in Fig. 1 in Ref. [13]). The primary ion beam and secondary target beam cross each other perpendicularly in the main chamber at the scattering center. For time-of-flight (TOF) measurements, the primary $^6Li^+$ ion beam [17] was pulsed with a pair of condenser plates [18]. Supersonic and capillary beams [13,19] were used as secondary beam in the experiments. The laboratory scattering angle θ is determined with respect to the primary ion-beam axis. The flight-path length from the scattering center to the detector is about 50 cm. The overall angular resolution for the scattered particle is about 0.12° full width at half maximum (FWHM). The time resolution $\Delta t/t$ in the TOF measurements is approximately 1/800 (FWHM) for an ion energy $E_{\rm lab}=500$ eV at a scattering angle $\theta=2°$. In this paper we will discuss only the dominant $^6Li^+$-^{20}Ne collisions.

In the apparatus used, both ions and neutral atoms scattered into an angle θ are simultaneously detected through a secondary-electron multiplier (Hamamatsu R595). Since a negative high voltage ($V_{\rm EM}=-2.7$ kV) is usually applied to the first dynode of the multiplier, the detection efficiency ε of the multiplier for the positive ions can be estimated to be unity. However, the efficiency ε for the neutral atoms is smaller than unity, when the impinging energy $E_{\rm im}$ is lower than a critical energy. In order to evaluate the correct intensity of the neutral particles, the efficiency ε (Li) for Li atoms has been experimentally determined within an uncertainty of 20% at the energies $140<E_{\rm im}<1000$ eV [13], i.e., ε(Li) $\simeq 0.1$ and 0.5 at $E_{\rm im}=150$ and 400 eV, respectively. ε (Ne) for Ne atoms has also been determined at $60<E_{\rm im}<1000$ eV in scattering experiments for K^+-Ne collisions [20]. The efficiencies ε (Li) and ε (Ne) are unity at energies $E_{\rm im}$ higher than 700 and 1000 eV, respectively.

B. Energy-transfer spectra

The TOF measurements have been performed at laboratory scattering angles of $2°\leqslant\theta\leqslant 92°$ and collision energies of $200\leqslant E_{\rm lab}\leqslant 500$ eV. In the TOF spectra, the scattered Li^+ ions and Li atoms and recoiled Ne atoms and Ne^+ ions have been observed. Furthermore an additional weak signal due to photons emitted from the excited Ne and Ne^+ has been found in the spectra. Since the recoiled Ne and Ne^+ belong to the same reaction channels as those of the scattered Li^+ and Li, here we will discuss the spectra for the Li^+ ions and Li atoms.

Figure 1 shows the energy-transfer spectra of the Li^+ ions and Li atoms at $E_{\rm lab}=500$ eV and $\theta=22°$, where the abscissa is the energy transfer Q from the kinetic energy to the internal energy of colliding particles in units of eV. These spectra are deduced from the TOF spectra by taking account of the Jacobian factor dQ/dt, where t is the flight time. The energy transfers Q for important exit channels are presented in Table I. The inelastic signal A_1 of the Li^+ ions in Fig. 1(a)

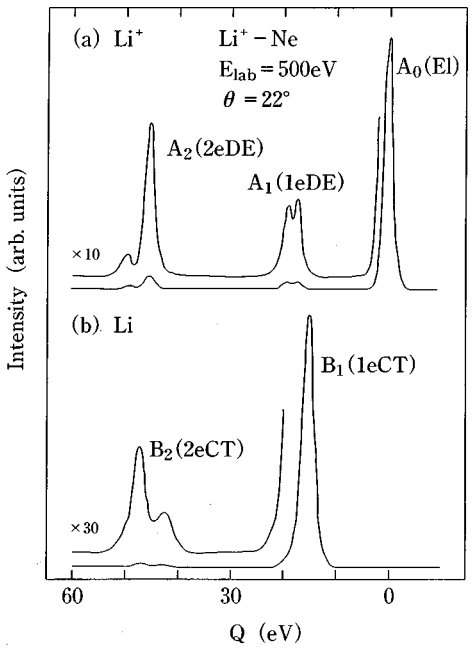

FIG. 1. Energy-transfer spectra in the Li^+-Ne collisions measured at $E_{\rm lab}=500$ eV and $\theta=22°$. (a) Spectrum of the Li^+ ions. Peak A_0 is ascribed to the elastic scattering (E1). Peaks A_1 and A_2 correspond to one- and two-electron excitations of Ne atoms (1eDE and 2eDE), respectively. (b) Spectrum of the Li atoms. Peaks B_1 and B_2 are due to one- and two-electron transitions (1eCT and 2eCT), respectively.

is composed of double peaks, and is ascribed to $1e$ direct excitations into the Ne($3s$) and Ne($3p$) states. Signal A_2 has a dominant peak located around $Q=45$ eV and a weak peak around $Q=48$ eV, and is attributed to $2e$ excitations of the Ne atoms into the autoionizing states of Ne$[2p^4(^1D)3s^2]$ with $Q=45.1$ eV, and Ne$[2p^4(^1S)3s^2]$ with $Q=48.3$ eV [5]. Atom signal B_1 in Fig. 1(b) is due to the $1e$ charge transfer into the Li($2s$)$+Ne^+$ state with $Q=16.2$ eV. Signal B_2 has double peaks located around $Q=43.5$ and 47.3 eV, and is ascribed to the charge-exchange reactions with target excitation into the states of Li($2s$)$+Ne^+[2p^4(^3P)3s]$ ($Q=44.0$ eV) and Li($2s$)$+Ne^+[2p^4(^1D)3s]$ ($Q=46.7$ eV) of $2e$ processes.

Figure 2 exhibits the energy-transfer spectra measured at $E_{\rm lab}=500$ eV and $\theta=40°$. Signal A_1 of the Li^+ ions located around $Q=19.5$ eV is attributed to $1e$ excitations into the Ne($3p$), Ne($4s$), and Ne($3d$) states. Signal A_2 is composed of double peaks located around $Q=45.5$ and 50.5 eV, and of a shoulder around $Q=55$ eV. The peak around $Q=45.5$ eV corresponds to $2e$ excitation into the $Li^+ +$Ne$[2p^4(^1D)3s^2]$ state, and the peak around $Q=50.5$ eV is mainly attributed to $2e$ excitation into states of Ne$[2p^4(^1D)3s3p]$ with $Q=48.9$ eV and Ne$[2p^4(^1D)3s3d]$ with $Q=50.0$ eV [5]. The shoulder around $Q=55$ eV will be attributed to the production of $Ne^+[2p^4(^1D)3p]$ ions ($Q=55.8$ eV). Signal B_1 of the Li atoms in Fig. 2(b) is composed of double peaks. The dominant peak is due to $1e$ charge transfer into the Li($2s$) $+Ne^+$ state, while the weak peak around $Q=20$ eV is due to products Li($3s$) and/or Li($3p$). Signal B_2 has also double

TABLE I. Energy transfers Q and relative intensity for important excitation processes in the Li^+-Ne collisions.

Exit channel	Q (eV)	Relative intensity
One-electron processes		
(1) Direct excitation	(Li^+ peak A_1)	
$Li^+ + Ne(3s)$	16.7	Low
$Li^+ + Ne(3p)$	18.7	Middle
$Li^+ + Ne(4s)$	19.7	Low
(2) Charge transfer	(Li peak B_1)	
$Li(2s) + Ne^+$	16.2	High
$Li(3s) + Ne^+$	19.5	Low
Two-electron processes		
(3) Direct excitation	(Li^+ peak A_2)	
$Li^+ + Ne[2p^4(^1D)3s^2]$	45.1[a]	Middle
$Li^+ + Ne[2p^4(^1D)3s3p]$	48.9[a]	Low
(4) Charge transfer	(Li peak B_2)	
$Li(2s) + Ne^+[2p^4(^1D)3s]$	46.7	Low
$Li(2s) + Ne^+[2p^4(^1D)3p]$	50.4	Low

[a]Olsen and Andersen (Ref. [5]).

peaks around $Q=47.5$ and 51 eV which are scarcely separated. The peak around $Q=47.5$ eV is mainly due to the charge transfer with target excitation into the $Li(2s)+Ne^+[2p^4(^1D)3s]$ state, and another peak around $Q=51$ eV is ascribed to the exit channel of $Li(2s)+Ne^+[2p^4(^1D)3p]$, with $Q=50.4$ eV. The broader structure in signal B_2, however, will indicate that the contribution of the excitation signals into $Li(2p)$, $Li(3s)$, and $Li(3p)$ states cannot be ignored.

Figure 3 shows angular dependence of the Li^+-ion peak A_1 for $1e$ excitation of the Ne atoms measured at $E_{lab}=500$ eV, where peak A_1 is presented with almost the same height. As shown in the figure, at small angle $\theta=17°$ signal A_1 is predominantly due to $Ne(3s)$ excitation, while at $\theta=30°$ the dominant signal is ascribed to the transition into the $Ne(3p)$ state. Thus the $1e$ direct excitation depends strongly on the scattering angle. The weak $2e$ excitation peaks located at 48 eV in signal A_2 and at 43.5 eV in signal B_2, shown in Fig. 1, have also been observed only at small angles of $\theta<30°$, similarly to the $Ne(3s)$ excitation.

All the energy-transfer spectra of the scattered Li^+ ions and recoiled Ne atoms measured at $\theta\leqslant 92°$ only have signals

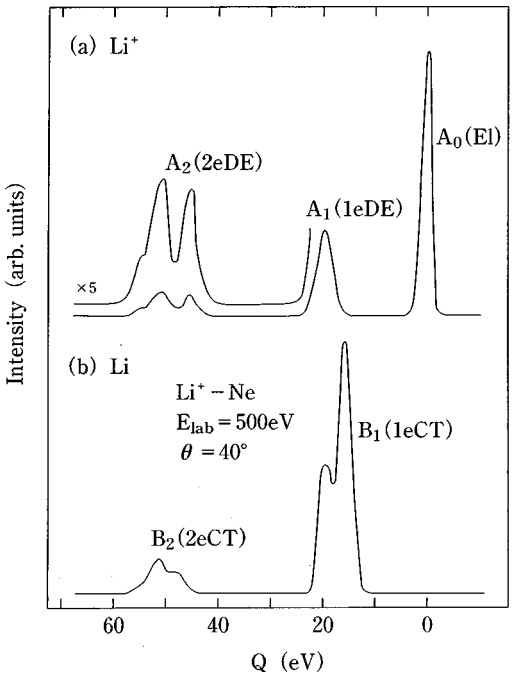

FIG. 2. Energy-transfer spectra of Li^+ ions and Li atoms measured at $E_{lab}=500$ eV and $\theta=40°$.

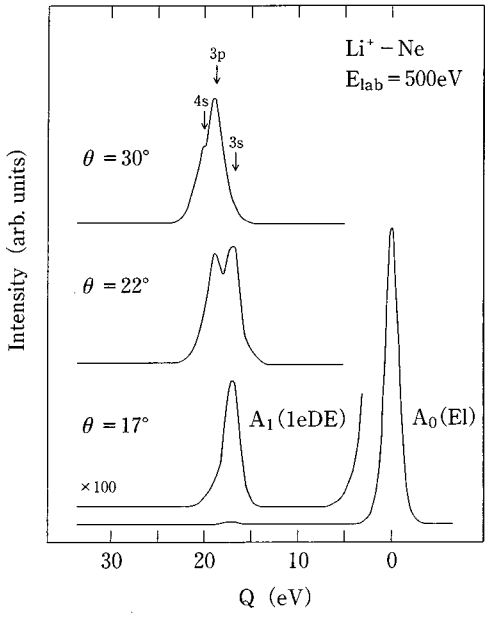

FIG. 3. Angular dependence of the Li^+ -ion peak A_1 for one-electron excitation of the Ne atoms (1eDE). Arrows $3s$, $3p$, and $4s$ indicate the energy-transfer locations for the $Ne^*(3s)$, $Ne^*(3p)$, and $Ne^*(4s)$ excitations, respectively.

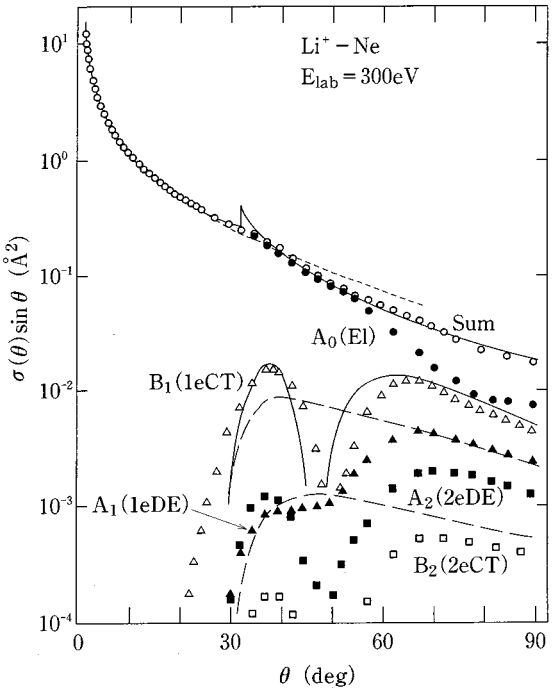

FIG. 4. Angular dependence of the DCS $\sigma(\theta)\sin\theta$ of the scattered Li^+ ions and Li atoms at $E_{lab}=300$ eV. ○ and ●: experimental summed DCS $\sigma(\theta)_{sum}$ and elastic DCS $\sigma(\theta)_{A0}$ for Li^+ peak A_0, respectively. △ and ▲: experimental DCS $\sigma(\theta)_{B1}$ for 1eCT (Li peak B_1) and DCS $\sigma(\theta)_{A1}$ for 1eDE (Li^+ peak A_1), respectively. □ and ■: experimental DCS $\sigma(\theta)_{B2}$ for 2eCT (Li peak B_2) and DCS $\sigma(\theta)_{A2}$ for 2eDE (Li^+ peak A_2), respectively. — — —: elastic DCS calculated using the experimental potential of Eq. (1). : DCS's $\sigma(\theta)_{sum}$ and $\sigma(\theta)_{B1}$ calculated with the two-state approximation. — —: DCS's $\sigma(\theta)_{B1}$ and $\sigma(\theta)_{A2}$ calculated with the four-state approximation.

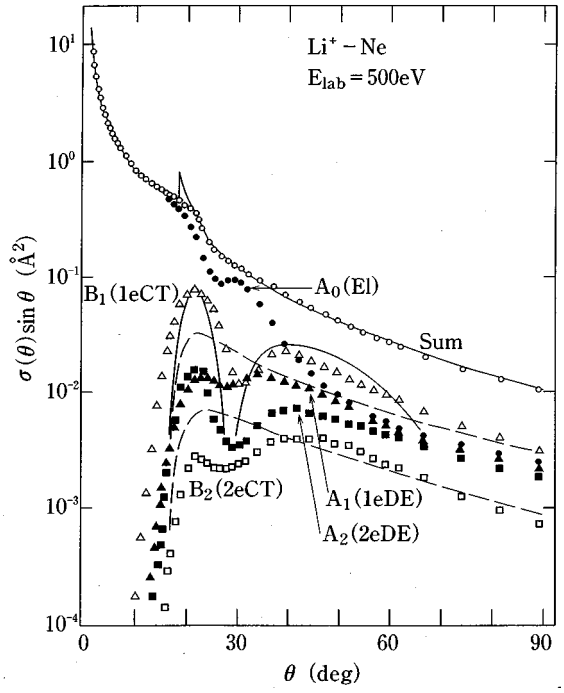

FIG. 5. Angular dependence of the DCS $\sigma(\theta)\sin\theta$ of the scattered Li^+ ions and Li atoms at $E_{lab}=500$ eV.

located at energy transfers of $Q<60$ eV and $Q<22$ eV, respectively. One can, therefore, conclude that excitation of Li^+ ions ($Q\geqslant 60.8$ eV) has very small probability under the experimental conditions in this study. In order to detect the negative Li^- ions produced in the collisions, additional TOF measurements, in which the first dynode of the multiplier was grounded, have also been performed at $E_{lab}=500$ eV and $\theta\leqslant 40°$. However, the Li^- ions could not be found in the TOF spectra.

C. Differential cross sections

Angular dependence of the DCS $\sigma(\theta)\sin\theta$, for the Li^+ ions and Li atoms scattered at $E_{lab}=300$ eV, is shown in Fig. 4. The elastic DCS $\sigma(\theta)_{A0}$ is presented only at large angles of $\theta>30°$ in the figure, because $\sigma(\theta)_{A0}$ is nearly equal to the summed DCS $\sigma(\theta)_{sum}$ at small angles. The $1e$ charge transfer DCS $\sigma(\theta)_{B1}$ is predominantly attributed to reaction into the $Li(3s)+Ne^+$ state, and the oscillatory structure in $\sigma(\theta)_{B1}$ is due to the interference between the different scattering trajectories. The $1e$ direct excitation DCS $\sigma(\theta)_{A1}$ also has double maxima, in which the first maximum around $\theta=40°$ is due to both the Ne($3s$) and Ne($3p$) excitations, as seen in the excitation signal A_1 in Fig. 1(a), while the second maximum around $\theta=70°$ is due to Ne excitations into $3p$ and $4s$ states. The origin of the double maxima in $\sigma(\theta)_{A1}$ seems to be different from that in $\sigma(\theta)_{B1}$. The $2e$ excitation DCS $\sigma(\theta)_{A2}$ is predominantly ascribed to reaction into the $Li^+ + Ne[2p^4(^1D)3s^2]$ state, with $Q=45.1$ eV. For this energy, the component A_2 with larger energy transfer of $Q\simeq 50$ eV, which can be seen in Fig. 2(a), was observed only at $\theta>80°$. The oscillatory structure in the DCS $\sigma(\theta)_{A2}$ is due to the interference effect. The charge transfer DCS $\sigma(\theta)_{B2}$ for a $2e$ process is so low that it could be scarcely measured by the TOF experiments with a poor time resolution at this energy.

Figure 5 exhibits the DCS $\sigma(\theta)\sin\theta$ at $E_{lab}=500$ eV. All excitation DCS's in the figure appear at nearly the same angle, and have double maxima. Since several exit channels contribute to each excitation DCS at large angles of $\theta>30°$ for this energy, the oscillatory structures in the DCS's $\sigma(\theta)_{B1}$ and $\sigma(\theta)_{A2}$ are somewhat obscure in comparison with those in Fig. 4 at $E_{lab}=300$ eV. As can be seen in Figs. 4 and 5, the dominant $1e$ and $2e$ excitations in the Li^+-Ne collisions near threshold are due to charge transfer and direct excitation of Ne atoms, respectively.

Since the DCS's measured in this study at $200\leqslant E_{lab}\leqslant 500$ eV are relative ones, the experimental summed DCS $\sigma(\theta)_{sum}$ at reduced angles $\tau=E_{lab}\theta<6.5$ keV deg, where the scattering is almost elastic, was normalized to the elastic DCS calculated by using the experimental potential

$$V(R)=1620\exp(-5.30R)\ \text{eV}, \tag{1}$$

where R is in units of Å [21].

III. ANALYSIS OF EXPERIMENTAL RESULTS

As shown in Figs. 4 and 5, the $1e$ charge transfer DCS $\sigma(\theta)_{B1}$ has the highest magnitude among the excitation DCS's, and shows a distinct oscillatory structure due to interference effect. Assuming interference between two different trajectories, angular spacing $\Delta\Theta$ of the oscillation is given by $\Delta\Theta = 2\pi/k\Delta b$, where Δb is the difference between the impact parameters leading to the same center-of-mass angle Θ, and k is the wave number [22]. The Δb originates from the difference between the diabatic ground- and excited-state potentials V_1 and V_2. Therefore, the oscillating structure provides us information on the potential difference $\Delta V = V_2 - V_1$. The excited-state potential V_2 for the $\mathrm{Li}(2s) + \mathrm{Ne}^+$ state as well as the ground-state potential V_1 was first evaluated by the fitting of the DCS $\sigma(\theta)_{B1}$, assuming a two-state approximation. The dominant $2e$ process is excitation into the autoionizing state of $\mathrm{Ne}^{**}(3s^2)$. Second, the potential for $\mathrm{Li}^+ + \mathrm{Ne}(2p^4 3s^2)$, as well as those for the ground and $1e$ excited states, were evaluated by fitting of the DCS's $\sigma(\theta)_{B1}$, $\sigma(\theta)_{A1}$, and $\sigma(\theta)_{A2}$, assuming a four-state approximation.

A. One-electron charge transfer

The experimental $1e$ charge transfer DCS $\sigma(\theta)_{B1}$ was analyzed semiclassically by employing the Landau-Zener transition probability modified by Zhu and Nakamura [15],

$$p = \exp(-2\pi V_{12}^2 f/\hbar v_r \Delta S), \tag{2a}$$

with

$$f = [2/(1+\sqrt{1+(0.70+0.40a^2)b^{-4}})]^{1/2}, \tag{2b}$$

where V_{12} is the interaction energy at the avoided-crossing point between the ground and excited states, v_r is the radial velocity, and ΔS is the difference in slopes of the two potential curves V_1 and V_2. The probability p must has a finite value even if the turning point R_0 coincides with the crossing distance R_c. The original Landau-Zener formula [23], however, gives $p=0$ at $R_0 = R_c$. The quantity f in Eq. (2) is a correction factor by Zhu and Nakamura, and a and b in the factor f are the diabatic parameters $(ab)^{-1} = 8V_{12}^2/\hbar v_r \Delta S$. In the fitting procedure, diabatic ground- and excited-state $[\mathrm{Li}(2s) + \mathrm{Ne}^+]$ potentials were initially estimated by referring to the pseudo-ground-state potential

$$V(R) = 1620\exp(-5.30R) - (12.212R)^{12}\exp(-38R)\ \mathrm{eV}, \tag{3}$$

which was evaluated from the experimental summed DCS $\sigma(\theta)_{\mathrm{sum}}$ in Figs. 4 and 5. Taking into account the interference effect, the semiclassical DCS $\sigma(\theta)_{B1}$ was calculated iteratively as a function of potential parameters and of the interaction energy V_{12}, to obtain a best fit of the experimental DCS $\sigma(\theta)_{B1}$. The solid curves in Figs. 4 and 5 give the best-fit results of the summed and $1e$ charge-transfer DCS's. The calculations reproduce the experiments at $200 \leqslant E_{\mathrm{lab}} \leqslant 500$ eV fairly well, except the DCS $\sigma(\theta)_{B1}$ at $\theta > 60°$ for $E_{\mathrm{lab}} = 500$ eV, where the two-state approximation will not be applicable. The diabatic ground- and excited-state potentials deduced from the experiments are

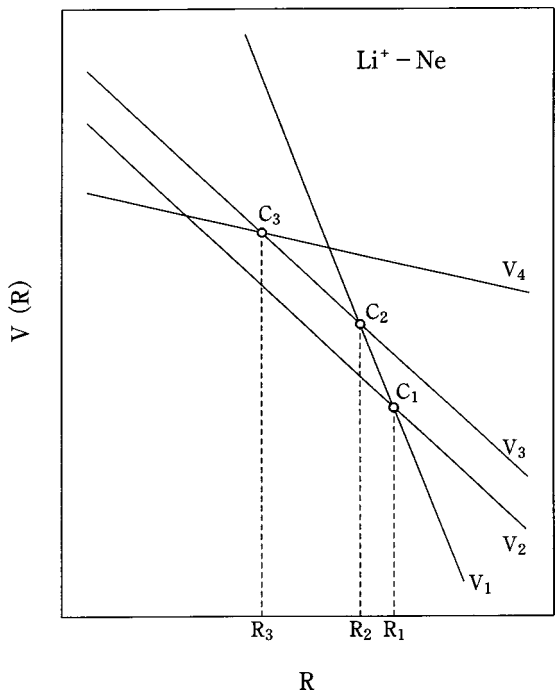

FIG. 6. Schematic drawing of the diabatic potentials used in the data analysis. The potential V_1 is for the ground state. The potentials V_2, V_3, and V_4 are for the excited states of $\mathrm{Li}(2s) + \mathrm{Ne}^+$, $\mathrm{Li}^+ + \mathrm{Ne}(3s)$, and $\mathrm{Li}^+ + \mathrm{Ne}(3s^2)$, respectively, at a separated distance. The electronic transitions are assumed to take place at the crossings C_1, C_2, and C_3.

$$V_1 = 1620\exp(-5.30R) - (11.892R)^{12}\exp(-38R)\ \mathrm{eV}, \tag{4a}$$

$$V_2 = 2045\exp(-6.05R) - (12.212R)^{12}\exp(-38R) + 16.2\ \mathrm{eV}. \tag{4b}$$

The potential parameters at the crossing point, which characterize the electronic transition, are $R_c = 0.554$ Å $[V(R_c) = 81.3\ \mathrm{eV}]$, $V_{12} = 3.10$ eV, and $\Delta S = 51.9$ eV/Å. The difference potential given by Eq. (4) is estimated to be meaningful at $R > 0.36$ Å.

B. Two-electron excitation of Ne atoms

Figure 6 shows a schematic drawing of the diabatic potential curves for Li^+-Ne employed in the analysis of the experimental DCS's, assuming a four-state approximation. Although some exit channels contribute to the $1e$ direct excitation DCS $\sigma(\theta)_{A1}$, as seen in Fig. 3, we have employed a potential curve V_3 for the $1e$ excited states of the Ne atoms. In the analysis, $1e$ charge transfer and $1e$ direct excitation were assumed to take place through crossings C_1 and C_2, respectively, and $2e$ excitation into the $\mathrm{Li}^+ + \mathrm{Ne}(3s^2)$ state was assumed to proceed through the crossing C_3 by two-step $1e$ transitions similarly to that for the quasisymmetric Na^+-Ne system [9,10(b)]. The excited-state potentials V_2,

TABLE II. The crossing parameters deduced from the experiments by assuming four-state approximation and from the MCSCF potentials.

Parameter	C_1	C_2	C_3
		Experiment	
R_c (Å)	0.582	0.574	0.529
$V(R_c)$ (eV)	78.3	81.8	98.4
V_{ij} (eV)[a]	3.55	2.80	2.80
$V_{ij}^2/\Delta S$ (eV Å)	0.192	0.112	0.090
ΣV_{ij} (eV)[b]	3.55	6.35	9.15
		MCSCF	
R_c (Å)	0.566	0.530	0.504
$V(R_c)$ (eV)	85.0	106	121
V_{ij} (eV)	3.50	1.90	2.63
$V_{ij}^2/\Delta S$ (eV Å)	0.21	0.080	0.067

[a] $V_{ij}=V_{12}$ for C_1, V_{13} for C_2, V_{34} for C_3, referring to Fig. 6.
[b] $\Sigma V_{ij}=V_{12}$ for C_1, $V_{12}+V_{13}$ for C_2, $V_{12}+V_{13}+V_{34}$ for C_3.

V_3, and V_4, as well as the ground-state potential V_1, were evaluated with the fitting of the excitation DCS's $\sigma(\theta)_{B1}$, $\sigma(\theta)_{A1}$, and $\sigma(\theta)_{A2}$, shown in Figs. 4 and 5. In the fitting procedure, the classical excitation DCS's were iteratively calculated without the interference effect as a function of the potential parameters and of the interaction energy V_{ij} at each crossing point.

The broken curves in Fig. 4 show the fitting results of the $1e$ charge transfer DCS $\sigma(\theta)_{B1}$ and the DCS $\sigma(\theta)_{A2}$ for $2e$ excitation of the Ne atoms. Since the excitation DCS's in the fitting procedure with the four-state approximation were calculated without the interference effect, the fitting results of $\sigma(\theta)_{B1}$ and $\sigma(\theta)_{A2}$ are approximately half that of the experiments around the maxima. As can be seen in Fig. 4, the agreement between the calculations and the experiments is reasonable. The calculated DCS $\sigma(\theta)_{A1}$ for $1e$ excitation of the Ne atoms is almost the same as the $\sigma(\theta)_{A2}$, and is not shown here for the sake of clarity. The fitting result of DCS $\sigma(\theta)_{A1}$ reproduces the experiments at $\theta<50°$ fairly well, but it does not at $\theta>50°$.

The broken curves in Fig. 5 for $E_{\rm lab}=500$ eV also represent the calculated excitation DCS's $\sigma(\theta)_{B1}$ and $\sigma(\theta)_{A2}$. The calculated $\sigma(\theta)_{A1}$, which is not shown here, is again nearly the same as the $\sigma(\theta)_{A2}$. The fitting result of DCS's $\sigma(\theta)_{B1}$ and $\sigma(\theta)_{A2}$ satisfactorily reproduce the experiments over the whole angular range. For the DCS $\sigma(\theta)_{A1}$, the fitting result fairly well reproduces the experiments around the first maximum, while at $\theta>30°$ the agreement between them is not enough. These results will suggest that the experimental DCS $\sigma(\theta)_{A1}$ can be satisfactorily reproduced only by taking into account additional potential curves for the $1e$-excited states of Ne$(4s)$ and Ne$(3d)$. The potential parameters at the crossings C_1, C_2, and C_3, deduced with the analysis, are summarized in Table II. The parameters at the crossing C_1 in the table are almost the same as those determined using the two-state approximation mentioned above.

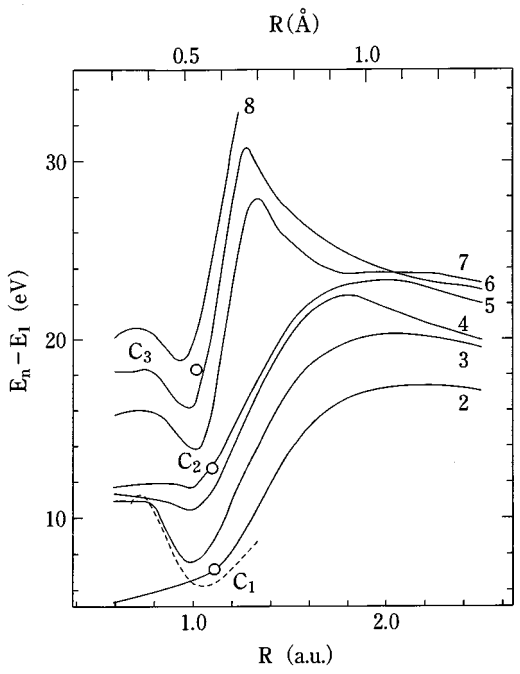

FIG. 7. Adiabatic difference potentials of the excited states. ——: MCSCF calculations. − − −: experimental potential for one-electron charge transfer. ○: experimental potentials at the crossing points C_1, C_2, and C_3.

IV. COMPUTATION OF INTERACTION POTENTIALS

For elucidation of the excitation mechanisms in the Li^+-Ne collisions near threshold, *ab initio* $^1\Sigma^+$ potentials of singly and doubly excited states, as well as the $^1\Sigma^+$ ground-state potential, have been calculated at internuclear distances of $0.6\leqslant R\leqslant 10$ a.u. with the MCSCF method. The calculations were carried out using the quantum-chemistry code GAMESS revised by Schmidt *et al.* [14]. The active space of the MCSCF computation includes all valence orbitals and electrons. In the calculations, we used the McLean-Chandler extended basis set [24] augmented by double sets of six *d* functions for Li and Ne atoms. The orbital exponents of the polarization functions are 0.1 and 0.4 for the Li atom, and 1.152 and 4.608 for the Ne atom. Our basis set has, therefore, the quality of triple ζ plus double polarizations.

The ground-state potentials calculated using the MCSCF method agree quite well with the experimental potential of Eq. (3) and the previous calculations [11,25,26], and also with the empirical model potential [27]. The solid curves in Fig. 7 show the adiabatic difference potentials of $\Delta E=E_n-E_1$ for Li^+-Ne calculated by the MCSCF method, where E_1 and E_n are the electronic energies for ground state 1 and excited state *n*, respectively. In this figure, we show only the potentials of the six lowest excited states and a highly excited state which are related to our discussion. Since the calculations were performed mostly with an interval of $\Delta R=0.1$ a.u. ($\Delta R=0.05$ a.u. at $0.9\leqslant R\leqslant 1.1$ a.u.), the curves in the figure are interpolated ones. The main configurations in the wave functions of states shown in Fig. 7 at the specific distances are listed in Table III. The configurations of excited states $n=3-7$ strongly depend on the distance at R

TABLE III. Main configurations in the MCSCF wave functions of states at specific distances of 0.9, 1.1, 2.2, and 10 a.u. In the configurations without superscripts a–d, the Ne $2p_z$ electron(s) is promoted into empty $n's$ or (/and) $n'p_z$ orbital(s), where the z axis is along the molecular axis.

	Distance R (a.u.)			
State	0.9	1.1	2.2	10
1	$Li^-(2s^2)+Ne^{2+}(2p^4)$	$Li^++Ne(2p^6)$ $Li(2s)+Ne^+(2p^5)$	$Li^++Ne(2p^6)$	$Li^++Ne(2p^6)$
2	$Li(2p)+Ne^+(2p^43s)$	$Li(2s)+Ne^+(2p^5)$ $Li^++Ne(2p^6)$	$Li(2s)+Ne^+(2p^5)$	$Li(2s)+Ne^+(2p^5)$
3	$Li(2s)+Ne^+(2p^5)$	$Li(2p)+Ne^+(2p^5)$	$Li(2p)+Ne^+(2p^5)$	$Li^++Ne(2p^53s)$
4	$Li^++Ne(2p^43s^2)$ $Li^++Ne(2p^53s)$	$Li^++Ne(2p^53s)$	$Li(2p)+Ne^+(2p^5)$[a]	$Li(2p)+Ne^+(2p^5)$[a]
5	$Li(2s)+Ne^+(2p^43p)$ $Li^++Ne(2p^53p)$	$Li^++Ne(2p^53p)$	$Li^++Ne(2p^53p)$[b]	$Li(2p)+Ne^+(2p^5)$
6	$Li^++Ne(2p^6)$ $Li(2p)+Ne^+(2p^5)$	$Li^-(2s^2)+Ne^{2+}(2p^4)$	$Li^++Ne(2p^53s)$	$Li^++Ne(2p^53p)$[b]
7	$Li^++Ne(2p^6)$ $Li(2p)+Ne^+(2p^5)$	$Li^-(2s2p)+Ne^{2+}(2p^4)$	$Li^++Ne(2p^53p)$	$Li^++Ne(2p^53p)$
8	$Li^-(2p^2)+Ne^{2+}(2p^4)$[c]	$Li^-(2s2p)+Ne^{2+}(2p^4)$	$Li(2s)+Ne^+(2s2p^6)$[d]	$Li(2s)+Ne^+(2s2p^6)$[d]

[a] $[Li(2p_x)+Ne^+(2p^62p_x^{-1})]+[Li(2p_y)+Ne^+(2p^62p_y^{-1})]$.
[b] $[Li^++Ne(2p^62p_x^{-1}3p_x)]+[Li^++Ne(2p^62p_y^{-1}3p_y)]$.
[c] $[Li^-(2p_x^2)+Ne^{2+}(2p^62p_z^{-2})]+[Li^-(2p_y^2)+Ne^{2+}(2p^62p_z^{-2})]$.
[d] Promotion of the Ne $2s$ electron.

$\geqslant$1.6 a.u., which can be partly seen in the table, and all states change their configurations at $0.9 \leqslant R \leqslant 1.1$ a.u. These features are attributed to the multiple avoided crossings.

In an avoided crossing between states i and j, the adiabatic difference potential $\Delta E = E_j - E_i$ is related to the diabatic potential $\Delta V = V_j - V_i$ by

$$\Delta E = 2\sqrt{(\Delta V/2)^2 + V_{ij}^2}, \tag{5}$$

where $\Delta E = 2V_{ij}$ and $\Delta V = 0$ at the crossing distance R_c [28]. The dotted curve in Fig. 7 exhibits the adiabatic difference potential $\Delta E = E_2 - E_1$ estimated from the experimental potentials of Eq. (4), with $V_{12} = 3.1$ eV. The experimental ΔE at small distances $R < 0.95$ a.u. (0.5 Å) is close to curve 3 rather than curve 2. The open circles C_1, C_2, and C_3 in Fig. 7 denote the adiabatic difference potential $\Delta E(R_c) = 2\Sigma V_{ij}$, evaluated approximately with the sum of the experimental interaction energies ΣV_{ij} given in Table II at the crossing points C_1, C_2, and C_3, respectively. This approximation is due to the fact that the difference potentials ΔE's around the crossings C_2 and C_3 in Fig. 6 evaluated independently in the similar way as for the $C_1(\Delta E = E_2 - E_1)$ are approximately given by $\Delta E = 2V_{ij}$ at a very short range of distances of $\Delta R = R_{C3} - R_{C1} = 0.05$ Å, which can be seen in the dotted curve of $\Delta E = E_2 - E_1$ in Fig. 7. The open circles C_1 and C_2 in Fig. 7 are on curves 2 and 5, respectively, while the open circle C_3 is located between curves 7 and 8.

V. DISCUSSION

Electronic transitions due to radial coupling proceed efficiently through interactions around the critical (crossing) distance R_c, where the adiabatic difference potential usually has a minimum value $\Delta E_{\min}$ [11,13,15]. By evaluating diabatic potential-parameters at a distance R_c from the MCSCF potential around $\Delta E_{\min}$, we will discuss the excitation mechanisms for the dominant $1e$ charge transfer and $2e$ excitation of Ne atoms near threshold angles.

A. One-electron charge transfer

As seen in Table III, both the configurations of states 1 and 2 at $R = 1.1$ a.u. are $Li^+ + Ne$ and $Li(2s) + Ne^+$, and the two states interchange their configurations around $R = 1.1$ a.u. These are the typical features of an avoided crossing, so the crossing distance of C_1^* between states 1 and 2 was crudely estimated to be $R_{C1}^* = 1.1$ a.u. (0.58 Å). Here the crossing C_1^* corresponds to C_1 in Fig. 6.

The charge-exchange reaction into the lowest excited state of $Li(2s) + Ne^+$ takes place through the transition onto potential curve 2 in Fig. 7. Although the MCSCF calculations certainly indicate an avoided crossing between states 1 and 2 around $R_{C1}^* = 0.58$ Å, curve 2 ($\Delta E_{12} = E_2 - E_1$) in Fig. 7 has no appreciable minimum around R_{C1}^*. This is attributed to the multiple crossings between states 1 and 2, and between states 2 and 3 at $R < R_{C1}^*$. In order to determine the crossing distance R_c from the difference potential ΔE_{12}, we have especially assumed that the extremum point in the gradient $\beta = |d \ln \Delta E_{12}/dR|$ corresponds to the distance R_c in a similar way as for the previous Li^+-Ar system [13]. In this case, the sharp peak in the curve of $1/\beta$ located at $R = 0.566$ Å was assigned to the crossing point of C_1, i.e., $R_{C1} = 0.566$ Å [$V(R_{C1}) = 85.0$ eV], $V_{12} = 3.50$ eV, and $V_{12}^2/\Delta S = 0.207$ eV Å. R_{C1} is close to $R_{C1}^* = 0.58$ Å, esti-

mated crudely from the R dependence of the configurations of states 1 and 2, and all the parameters at the crossing C_1 deduced from the MCSCF potentials satisfactorily reproduce the experiments as shown in Table II. The $1e$ charge transfer into the $Li(2s)+Ne^+$ state, thus, can be well interpreted to occur through the avoided crossing between states 1 and 2. As shown by the dotted curve in Fig. 7, however, at smaller distances of $R<0.5$ Å, the experimental difference potential ΔE_{12} evaluated from the diabatic potentials of Eq. (4) close to curve 3 rather than curve 2. As a next step, we will discuss the transition from curve 2 onto curve 3 at $R<R_{C1}$.

The potential parameters at the crossing between states 2 and 3 were evaluated from the difference potential ΔE_{23}. The result is $R_c=0.53$ Å, $V_{23}=0.45$ eV, and $V_{23}^2/\Delta S=0.0082$ eV Å. Because of the small value of $V_{23}^2/\Delta S$, most of the particles diabatically path through the crossing from curve 2 onto curve 3. This is the reason why the experimental ΔE_{12} in Fig. 7 reproduces the MCSCF potential ΔE_{13} rather than the MCSCF ΔE_{12} at $R<0.5$ Å.

State 3 in Fig. 7, which has the configuration of $Li(2p)+Ne^+$ at $R=0.58$ Å (1.1 a.u.), as shown in Table III, adiabatically correlates to the $Li^+ + Ne(3s)$ state at the separated distance. Emergence of the particles along the adiabatic curve 3 results in $Ne(3s)$ excitation. The experimental finding that $Ne(3s)$ excitation could be observed only near the threshold angles, as seen in Fig. 3, can also be attributed to the small diadatic parameter of $V_{23}^2/\Delta S$.

B. Two-electron excitation of Ne atoms

1. First process in two-successive transitions

Excitation into the $Li^+ + Ne[2p^4(^1D)3s^2]$ state is considered to proceed through two successive $1e$ transitions, i.e., $Ne \rightarrow Ne^*(3s) \rightarrow Ne^{**}(3s^2)$ [9,10(b)]. The wave function of state 4 has a configuration of $Li^+ + Ne(3s)$ around the distance $R=0.58$ Å (1.1 a.u.), which can be seen in Table III. The configuration mixing of $Li^+ + Ne(3s)$ and $Li^+ + Ne(3s^2)$ in the wave functions of state 4 at $R=0.9$ (and 0.95) a.u. in Table III is considered to be ascribed to the avoided crossing C_3^* between the $1e$ and $2e$ excited states, i.e., $R_{C3}^* \simeq 0.93$ a.u. (0.49 Å). The transition onto curve 4 at $R<R_{C1}$ is, then, ascribed to the first process in the two-step $1e$ transitions. Here we will discuss the transition onto curve 4, which leads the excitation into the $Ne(3p)$ state.

Assuming the particles diabatically path through the crossing between states 2 and 3, the potential parameters at the crossing ($R_c<R_{C1}=0.57$ Å) for direct transition from state 2 into state 4 were evaluated from the difference potential ΔE_{24}. This approximation corresponds to the experimental analysis by assuming a potential V_3 for the $1e$ excited states of the Ne atoms as shown in Fig. 6, and provides the potential parameters at the crossing C_2. The results are $R_{C2}=0.530$ Å [$V(R_{C2})=106$ eV], $V_{24}=1.90$ eV, and $V_{24}^2/\Delta S=0.080$ eV Å. These values reasonably reproduce the experiments, as can be seen in Table II.

As shown in Table III, the wave function of state 4, which has the configuration $Li^+ + Ne(3s)$ at $R=0.58$ Å (1.1 a.u.), adiabatically correlates to $Li(2p)+Ne^+$ around $R=1.2$ Å (2.2 a.u.). At $R=1.2$ Å, state 6 has the configuration of $Li^+ + Ne(3s)$. MCSCF calculations show that there are successive avoided crossings at $0.85<R<1.2$ Å ($1.6<R<2.2$ a.u.) between states 4 and 5, and between states 5 and 6. According to the analysis of ΔE_{45} and ΔE_{56}, most particles going out along potential curve 4 pass the crossings ($p \simeq 0.9$) to curve 5 at $R_c \simeq 0.88$ Å, and further to curve 6 at $R_c \simeq 1.14$ Å. These successive transitions followed by the outgoing path along adiabatic curve 6 result in excitation into the $Li^+ + Ne(3p)$ state. The $Ne^*(3p)$ excitation observed experimentally at small angles is, then, attributed mainly to the transition onto curve 4 in Fig. 7 at $R_{C2}=0.53$ Å.

2. Second process in two-successive transitions

The $2e$ excitation into the $Ne(3s^2)$ state is ascribed to take place through the transition from state 4 to a state lying at a higher-energy level. The adiabatic difference potential at the crossing point C_3, estimated experimentally, which is indicated by an open circle in Fig. 7, is located between curves 7 and 8. As the R dependence of the MCSCF calculations suggests that $2e$ excitation occurs through the transition from state 4 into state 7, the potential parameters at the diabatic crossing were evaluated from $\Delta E_{47}=E_7-E_4$. The result is $R_c=0.504$ Å [$V(R_c)=121$ eV], $V_{47}=2.63$ eV, and $V_{47}^2/\Delta S=0.067$ eV Å, which are presented in Table II, and agree reasonably with the experiments for the crossing C_3. Since curve 7 leads adiabatically to the exit channel of $Li^+ + Ne(3p)$, the $2e$ excitation must be followed by a diabatic transition onto another potential curve lying at the higher-energy level, which leads to the exit channel of $Li^+ + Ne(2p^4 3s^2)$.

As discussed above, the configuration mixing of $Li^+ + Ne(3s)$ and $Li^+ + Ne(3s^2)$, in the wave functions of state 4 at $R_{C3}^*=0.49$ Å (0.93 a.u.) is attributed to the avoided crossing between the $1e$ and $2e$ excited states. The experimental result for $2e$ excitation, however, is interpreted by the transition from curve 4 onto curve 7 at $R_c=0.504$ Å (0.952 a.u.). The discrepancy suggests that the transition onto curve 7 is not the usual avoided crossing, but is due to a noncrossing interaction at the critical distance R_c, where two adiabatic potentials close in on each other, analogously to the transition in the Li^+-Ar collisions [11,13]. A careful analysis of the MCSCF potentials for $1e$ charge transfer due to the noncrossing interaction in Li^+-Ar has shown that the diabatic crossing distance R_c does not coincide with $R_{\min}$, where the adiabatic difference potential has a minimum value $\Delta E_{\min}$ [13]. The difference $\Delta R=R_c-R_{\min}$ depends on the curvature of ΔE around $R_{\min}$. Since the curvature of ΔE_{47} around $R_{\min}$ for Li^+-Ne is about a factor of 3 larger than that for Li^+-Ar, the ΔR for Li^+-Ne is expected to be sufficiently small. This will be the reason why the diabatic parameter $V_{47}^2/\Delta S$, evaluated from ΔE_{47}, satisfactorily agrees with the experiments.

The $2e$ excitation into the $Ne(3s^2)$ state has also been studied experimentally and theoretically for moderate-energy Na^+-Ne collisions [9,10(b)]. Theoretical analysis shows that

the excitation is well interpreted by the two successive $1e$ transitions occurring only through the avoided-crossing interactions [9]. This result for the quasisymmetric Na^+-Ne system is in contrast to that for the asymmetric Li^+-Ne.

In this study, experimental results near threshold angles have been analyzed by assuming only radial coupling, but excitations into the higher-energy levels observed at large angles must be analyzed by taking into account rotational coupling in addition to radial coupling.

C. Potential crossings

The gross features of the diabatic potential crossings for $1e$ and $2e$ excitations in the $Li^+ + Ne$ collisions can be qualitatively interpreted by the crossings of the promoted $3d\sigma$ molecular orbital around $R = 1.0$ a.u. evaluated by an *ab initio* calculation [11]. The MCSCF potentials calculated in this study, however, are different from the correlation energy diagram [6,11] deduced using the empirical electron-promotion model [29]. This suggests that a careful treatment is necessary to discuss the details of the excitation mechanisms. The origin of the potential crossings can also be intuitively interpreted by using the empirical charge-overlap model [27].

VI. SUMMARY

One- and two-electron excitations in the Li^+-Ne collisions were observed at the reduced angles at $E_{lab}\theta > 6$ keV deg at collision energies of $E_{lab} \geqslant 200$ eV. Among the excitations, $1e$ charge transfer into the $Li(2s) + Ne^+$ state has the highest transition probability. A remarkable excitation into the autoionizing $Ne^{**}(3s^2)$ state has also been observed in the experiments. The analysis of the experimental DCS's shows that the electronic transitions take place at the distances $R \leqslant 0.57$ Å. The excitations near the threshold could be well interpreted by the *ab initio* MCSCF potentials. The analysis of the MCSCF potentials indicates that $1e$ excitations are due to the usual avoided-crossing interactions, while the $2e$ excitation taking place through two successive $1e$ transitions is attributed to both the avoided-crossing and noncrossing interactions.

ACKNOWLEDGMENTS

We are grateful to Dr. H. Tanuma (Tokyo Metropolitan University, Tokyo, Japan) for his contribution to this work. This work was financially supported in part by the Matsuo Foundation, and by Grants-in-Aid for Scientific Research from the Ministry of Education, Science, and Culture of Japan.

[1] N. F. Mott and H. S. W. Massey, *The Theory of Atomic Collisions* (Oxford University Press, Oxford, 1965), Chaps. XIII and XXI.
[2] J. C. Mouzon, Phys. Rev. **41**, 605 (1932).
[3] D. C. Lorents and G. M. Conklin, J. Phys. B **5**, 950 (1972).
[4] V. P. Belik, S. V. Bobashev, and S. P. Dmitriev, Zh. Eksp. Teor. Fiz. **67**, 1674, (1974) [Sov. Phys. JETP **40**, 833 (1975)].
[5] J. Ø. Olsen and N. Andersen, J. Phys. B **10**, 101 (1977).
[6] B. I. Kikiani, R. A. Lomsadze, N. O. Mosulishvili, M. R. Gochitashvili, and V. M. Lavrov, Zh. Eksp. Teor. Fiz. **98**, 95 (1990) [Sov. Phys. JETP **71**, 51 (1990)].
[7] J. C. Brenot, D. Dhuicq, J. P. Gauyacq, J. Pommier, V. Sidis, M. Barat, and E. Pollack, Phys. Rev. A **11**, 1245 (1975).
[8] V. V. Afrosimov, Yu. S. Gordeev, and V. M. Lavrov, Zh. Eksp. Teor. Fiz. **68**, 1715 (1975) [Sov. Phys. JETP **41**, 860 (1976)].
[9] J. Ø. Olsen, T. Andersen, M. Barat, Ch. Courbin-Gaussorgues, V. Sidis, J. Pommier, J. Agusti, N. Andersen, and A. Russek, Phys. Rev. A **19**, 1457 (1979).
[10] (a) S. Kita, M. Izawa, and H. Inouye, J. Phys. B **16**, L499 (1983); (b) S. Kita, H. Tanuma, and M. Izawa, *ibid.* **20**, 3089 (1987).
[11] M. Barat, D. Dhuicq, R. Francois, and V. Sidis, J. Phys. B **6**, 2072 (1973).
[12] S. Kita, T. Hasegawa, H. Tanuma, and N. Shimakura, Phys. Rev. A **52**, 2070 (1995).
[13] S. Kita and N. Shimakura, Phys. Rev. A **55**, 3504 (1997).
[14] M. W. Schmidt, K. K. Baldridge, J. A. Boatz, S. T. Elbert, M. S. Gordon, J. H. Jensen, S. Koseki, N. Matsunaga, K. A. Nguyen, S. Su, T. L. Windus, M. Dupuis, and J. A. Montgomery, Jr., J. Comput. Chem. **14**, 1347 (1993).
[15] C. Zhu and H. Nakamura, J. Chem. Phys. **102**, 7448 (1995).
[16] H. Inouye, M. Izawa, S. Kita, K. Takahashi, and Y. Yamato, Bull. Res. Inst. Sci. Meas. Tohoku Univ. **32**, 41 (1984).
[17] S. Kita, S. Furusawa, H. Tanuma, I. Kusunoki, and M. Ishigame, Bull. Res. Inst. Sci. Meas. Tohoku Univ. **37**, 33 (1988).
[18] S. Kita and H. Inouye, J. Mass Spectrom. Soc. Jpn. **41**, 211 (1993).
[19] M. Izawa, S. Kita, and H. Inouye, J. Appl. Phys. **53**, 4688 (1982).
[20] S. Kita, S. Gotoh, N. Shimakura, and M. Izawa (unpublished).
[21] H. Inouye and S. Kita, J. Phys. Soc. Jpn. **34**, 1588 (1973).
[22] R. E. Olson and F. T. Smith, Phys. Rev. A **3**, 1607 (1971).
[23] L. D. Landau, Phys. Z. Sowjetunion **2**, 46 (1932); C. Zener, Proc. R. Soc. London, Ser. A **137**, 696 (1932).
[24] A. D. McLean and G. S. Chandler, J. Chem. Phys. **72**, 5639 (1980).
[25] Y. S. Kim and R. G. Gordon, J. Chem. Phys. **60**, 4323 (1974); V. K. Nikulin and Yu. N. Tsarev, Chem. Phys. **10**, 433 (1975).
[26] I. Røeggen and H. R. Skullerud, J. Phys. B **25**, 1795 (1992).
[27] S. Kita, S. Gotoh, T. Hasegawa, and N. Shimakura, J. Chem. Phys. **109**, 9713 (1998).
[28] G. Herzberg, *Molecular Spectra and Molecular Structure I. Spectra of Diatomic Molecules* (Van Nostrand Reinhold, New York, 1950), p. 283.
[29] M. Barat and W. Lichten, Phys. Rev. A **6**, 211 (1972).